Thin Solid Films 519 (2011) 7638–7643

Contents lists available at ScienceDirect

Thin Solid Films

journal homepage: www.elsevier.com/locate/tsf

Characterization of nanostructures of ZnO and ZnMnO films deposited by successive ionic layer adsorption and reaction method

F.N. Jiménez-García [a,b], D.G. Espinosa-Arbeláez [c,d], C. Vargas-Hernández [b], A. del Real [c], M.E. Rodríguez-García [c,*]

[a] Departamento de Física y Matemáticas, Universidad Autónoma de Manizales, Antigua Estación del Ferrocarril, Manizales, Caldas, Colombia
[b] Departamento de Física y Química, Universidad Nacional de Colombia, Sede Manizales, Campus la Nubia, Manizales, Caldas, Colombia
[c] Departamento de Nanotecnología, Centro de Física Aplicada y Tecnología Avanzada, Universidad Nacional Autónoma de México, Blv.Juriquilla 3001, Juriquilla, Querétaro, C.P. 76230, Mexico
[d] Posgrado en Ciencia e Ingeniería Materiales, Instituto de Investigación en Materiales, Universidad Nacional Autónoma de México, México DF, Mexico

ARTICLE INFO

Article history:
Received 16 April 2010
Received in revised form 9 May 2011
Accepted 10 May 2011
Available online 18 May 2011

Keywords:
Zinc oxide
Zinc manganese oxide
Scanning Electron Microscopy
Surface morphology
Atomic Force Microscopy
Nanostructured materials

ABSTRACT

ZnO and ZnMnO thin films were obtained by the successive ionic layer adsorption and reaction (SILAR) method. All thin films were deposited on glass microscope slide. A precursor solution of 0.1 M of $ZnCl_2$ complexed with ammonium hydroxide and water close to boiling point (92 °C) as a second solution was used for the ZnO films. An uncomplexed bath comprised of 0.1 M $ZnCl_2$, 0.1 M $MnCl_2$, and a second solution of 0.1 ml of NH_4OH with water close to boiling point was used for the ZnMnO films. The film samples were deposited by the SILAR method and annealed at 200 °C for 15 min. These samples were characterized using X-Ray Diffraction (XRD), Scanning Electron Microscopy with Energy Dispersive Spectroscopy (EDS), and Atomic Force Microscope. Atomic absorption was used to determine quantitatively the amount of Mn incorporated into the films. According to the XRD patterns these films were polycrystalline with wurtzite hexagonal structure. The morphology of the ZnO films constituted by rice-like and flower-like structures changed significantly to nanosheet structures with the Mn incorporation. The Mn inclusion in a ZnO structure was less than 4% according to the results from EDS, XRD, and atomic absorption.

© 2011 Elsevier B.V. All rights reserved.

1. Introduction

ZnO is a semiconductor of great interest because it has a band gap of 3.37 eV at room temperature with applications in optoelectronic devices emitting blue-violet light. It also exhibits characteristics suitable for additional technological applications such as antireflection coatings, transparent electrodes in solar cells, electronic and piezoelectric devices, and gas sensors, among others [1–6].

Another important feature of this material is the ability to incorporate transition metals such as Cr, V, Mn, Fe, Co into conventional semiconductor compounds which is important for the fabrication of diluted magnetic semiconductors (DMS). While many researchers concentrate on epitaxial doping, some other researchers employ methods such as ion implantation to incorporate magnetic impurities in semiconductors. DMS using ZnO doped with transitional metals are important and of great interest because of their technological applications due to their properties such as excellent optical emission, piezoelectric effect, field emission, and non-toxic effects [7,8]. Mn-doped ZnO film is a promising candidate because its ferromagnetism at room temperature has been theoretically predicted [9] for this material. Different methods have been used to prepare DMS such as molecular beam epitaxy [10–12], metal-organic chemical vapor deposition [13–15], magnetron sputtering [16–18], pulsed laser deposition [19–22], and sol–gel [23–26], among others.

Other simple, economical and effective techniques known as chemical bath deposition (CBD) and SILAR have been used to dope ZnO films with Cd, Cu, Al, and Ni [27–29]. However, there are no reports of Mn-doped ZnO films using this technique due to the difficulty in the formation of Mn complexes [30]. Two-dimensional nanomaterials such as nanobelts and nanosheets have recently attracted much attention because it was reported that ZnO nanosheets have better performance than nanorods as photocatalysts due to their large specific surface area and high population of polar faces [31,32]. Although two-dimensional DMS nanomaterials using ZnO could find application in other fields different from spintronics, the fabrication of nanosheets has been reported only by electrodeposition and CBD method showing room-temperature ferromagnetism by co-doping with Mn and Ni [33].

In this paper, we report the synthesis and characterization of ZnO and ZnMnO films grown by the SILAR method. The films were characterized by X-ray diffraction (XRD), Scanning Electron Microscope (SEM), Atomic absorption, Atomic Force Microscopy (AFM), Energy-Dispersive X-ray Analysis (EDX) and Differential Scanning Calorimetry (DSC).

* Corresponding author. Tel.: +52 442 2381141; fax: +52 442 2381165.
E-mail address: marioga@fata.unam.mx (M.E. Rodríguez-García).

0040-6090/$ – see front matter © 2011 Elsevier B.V. All rights reserved.
doi:10.1016/j.tsf.2011.05.008

2. Experimental details

2.1. Deposition method

Two ZnO and two ZnMnO films were deposited on a glass microscope slide by SILAR process. All substrates were treated before deposition as follows: they were boiled in dilute sulfuric acid (1:10 v/v) for 1 h. Then, they were ultrasonically rinsed in ethanol and acetone for 30 min. Finally they were stored in double deionized water until the moment of using them. For the growth of ZnO films, two solutions were used: the first solution consisted of 0.1 M $ZnCl_2$ and ammonium hydroxide (29%) solution as complexing agent, in molar ratio 1:10 at room temperature, and a second solution containing hot water close to boiling point. For the growth of ZnMnO films, two solutions were used: the first solution was of 0.1 M $ZnCl_2$ as a source of zinc and of 0.1 M $MnCl_2$ as a source of Mn, heated at 70 °C. The complexed solution commonly used in the case of ZnO deposition [34–36] was not employed due to the problem of $MnCl_2$ complex formation. The second solution was deionized water with concentrated ammonium hydroxide (29%) solution in volume ratio 1:30 heated at 85 °C.

Fig. 1 shows the experimental setup used to grow these thin films. A stepper motor was used to have a constant speed for the sample immersion in the chemical baths. This system allows the growth of four samples at the same time under the same conditions. Glass substrates were successively immersed in a first solution for 2 s at constant speed of 4 cm/s, which guarantees the deposition on the substrate. This was followed by the substrate being dipped in a second solution for 2 s. A manual rotation was used to stir both solutions. Using this semi-automatic procedure a reaction between Zn^{2+}, Mn^{2+} cations and O^{2-} anion took place on the surface of the substrate and films of ZnMnO or ZnO were deposited. One hundred and fifty deposition cycles were performed to obtain ZnMnO and ZnO layers. Samples were dried in current air for 1 h. Next, samples were annealed in air using a tube furnace 21100 (Thermolyne) and heated at 6 °C/min until they reached 200 °C. Finally, the samples remained at 200 °C for 15 min.

2.2. Characterization techniques

The ZnO and ZnMnO samples were measured in a DSC Q2000 V24.4 Build 116 (TA Instrument) in a closed aluminum cell, using a heating rate of 10 °C/min under nitrogen atmosphere at 60 ml/min with a mass average of samples of 8.5 mg. The objective was to evaluate the heat flow. The as-deposited and annealed ZnO as well as ZnMnO films were characterized by the following techniques: X ray diffraction patterns were obtained in the range of the diffraction angle between 15 and 80° in 2θ scale with CuK_α radiation and a Siemens D5000 diffractometer ($\lambda = 1.5406$ Å). Data were collected with 2 deg/min steps at room temperature. The aim was to study the structural transformation due to the annealing process. Using a JEOL JSM-6060 LV (Japan), Scanning Electron Microscope with the energy of 15 kV was used to study the morphology of samples. Semi-quantitative chemical compositions of thin films were obtained by means of an INCA Oxford-X ray Energy Dispersive Spectroscopy (EDS) at 20 KV. A Park Scientific Instrument atomic force microscope (AFM) was used to investigate the surface morphology of the films. Non-contact mode was used to measure ZnMnO and contact mode was used for ZnO film; the scanning area was 10×10 µm. Atomic absorption experiments were conducted to examine the amount of Mn incorporating into the ZnMnO films.

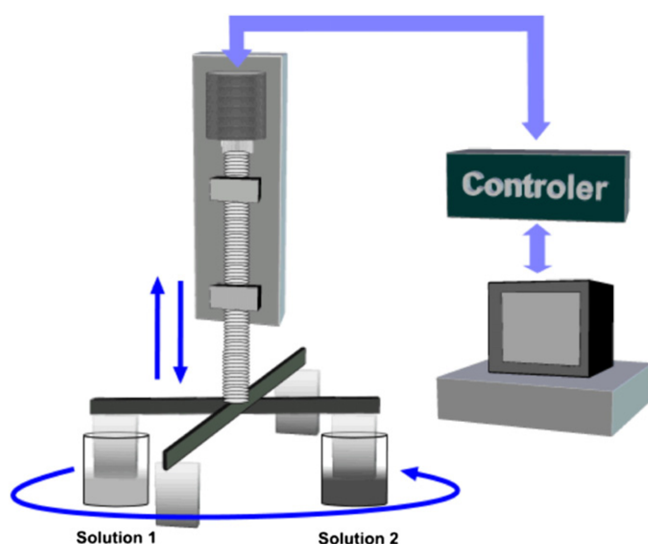

Fig. 1. Experimental setup used to grow ZnO and ZnMnO films.

3. Results and discussions

3.1. Differential scanning calorimetry analysis

One of the main problems with the growth of ZnO thin films under equilibrium conditions is their poor crystalline quality. Therefore, it is necessary to perform thermal treatments to produce structural changes in order to improve crystalline quality. To obtain the transition temperature for the thermal treatments of the samples, a differential scanning calorimetry (DSC) experiment was carried out. Fig. 2a shows the heat flow as a function of the temperature for ZnO sample. This figure clearly shows the presence of an endothermic peak around 94 °C, which is related to the water being removed from the matrix. Two small endothermic reactions can be detected at 132 and 157 °C. The first peak could be related to the transformation of $Zn(OH)_2$ into ZnO. This transformation occurs above 125 °C [37]. The second peak could be related to the volatile compounds of ammonium hydroxide [38]. Fig. 2b shows the heat flow as a function of the temperature for ZnMnO. An endothermic peak around 171 °C could be related to the hydroxide decomposition to their corresponding manganese oxides. A small peak around 140 °C could be related to the evaporation of chemically bound water [39]. An endothermic peak around 197 °C observed is possibly related to an improvement of the crystalline phase of the Simonkolleite ($ZnCl_2.4Zn(OH)_2.H_2O$) structure. This assumption is corroborated by XRD pattern taken before and after annealing treatment. This will be discussed later on. The Simonkolleite presence is possibly due to both the precursor $ZnCl_2$ employed and the formation of zinc hydroxide during the growth process [40,41]. The process was conducted in an aqueous solution.

3.2. XRD studies

Fig. 3 shows the XRD pattern of ZnO film as deposited and after annealing at 200 °C. According to the XRD patterns it is a polycrystalline film. The main crystalline orientation identified according to the JCPDS standard (No. 36–1451) data of wurtzite (hexagonal) ZnO powder were (100), (002), (101), (102), (110), (103), (112), (201), and (004). As it is typical of the XRD pattern, the presence of a mechanical stress can be detected by a broadening of the diffraction peaks. On the other hand, shift peaks to low angle in terms of the Bragg law consist of an increase of the interplanar distance due to inclusion of Mn [42]. A detailed inspection of each of the peaks for ZnO shows that when using the SILAR processes this structure does not have any mechanical stress [43]. Fig. 4a shows the XRD patterns of ZnMnO as deposited and ZnMnO after annealing at 200 °C. As a result of the annealing at 200 °C, the γ-$Zn(OH)_2$ phase identified by this pattern with JCPDS file No. 020–1435 and the β-$Zn(OH)_2$ identified with JCPDS No. 038–0356, were converted to ZnO, as it was confirmed by DSC thermogram. According to these patterns after annealing, the

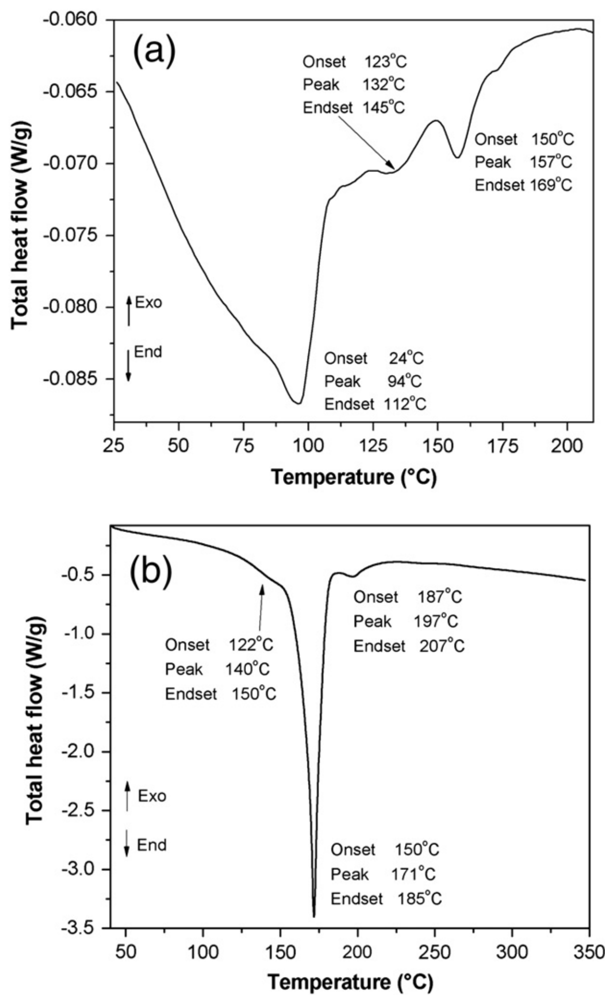

Fig. 2. Total heat flow as a function of the temperature (a) for ZnO film, and b) for ZnMnO film.

Simonkolleite phase was clearly identified with JCPDS No. 007–0155. The formation of ZnO was identified in this film. Diffraction peaks from crystal planes such as (100), (002), (101), (102), (110), (103), (112), and (201) were observed. All those peaks can be indexed to wurtzite hexagonal structure of ZnO (JCPDS No. 00 036 1451). No indications of Mn or manganese oxide were observed. The radius of

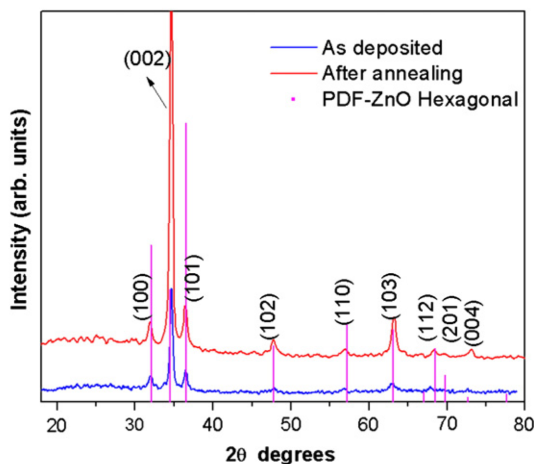

Fig. 3. XRD pattern for ZnO films as deposited and after annealing.

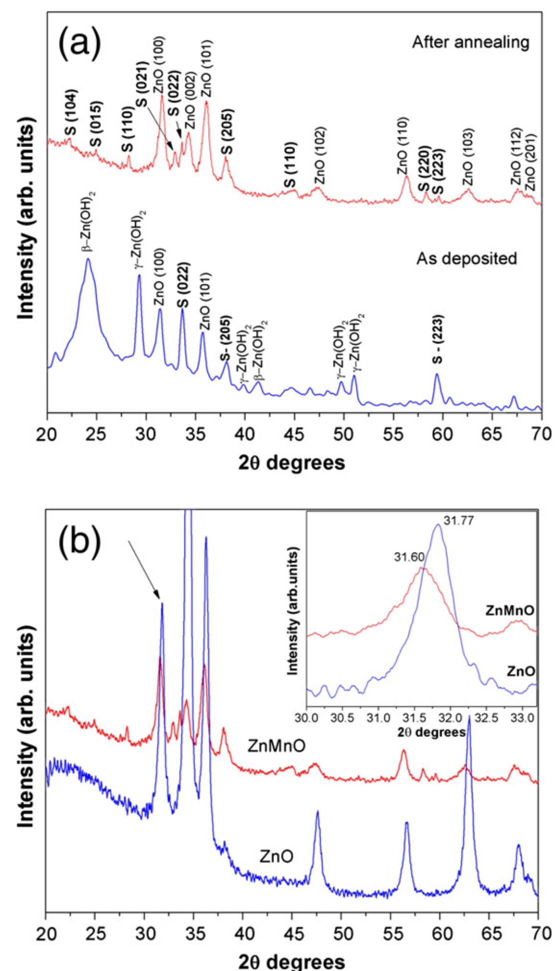

Fig. 4. XRD pattern as deposited and after annealing a) for ZnMnO films, and b) for ZnO and ZnMnO films. The inset shows the shift of the market peaks due to Mn incorporation.

Mn^{2+} (0.66 Å) is slightly larger than that of Zn^{2+} (0.60 Å). This generates the shift of XRD peaks to the left and the lattice enhancement because of its higher size. The incorporation of Mn in ZnO films was corroborated by the shift of peaks in the pattern and the increase of lattice parameter. The lattice parameters *a* and c of all DMS ternary alloys obey Vegard's law very closely [44]. Thus, by knowing the lattice parameters for ZnO and ZnMnO films it is possible to know the amount of Mn that it is being incorporated into the ZnO structure. Fig. 4b. shows the shift of XRD peaks of ZnMnO compared with ZnO. This type of shift has been reported by some authors [25]. Table 1 shows *a* and *c* values obtained from XRD patterns and the full width at half maximum (FWHM) for the (002) peak. According to some other authors, the hypothetical hexagonal MnO has $d = 3.25$ Å [13], then $a = 3.753$ Å and by Vegard's law, approximately 3.6% of Mn is incorporated into the ZnO structure. It is observed that the FWHM for the ZnMnO film increased in relation to the ZnO film as shown in Table 1. The ZnO film loses crystalline quality because of the incorporation of Mn.

Table 1
The lattice parameters (a and c), interplanar spacing (d) and FWHM evaluated from XRD patterns for ZnO and ZnMnO films.

Parameters	a (Å)± 0.007	c (Å)± 0.007	FWHM (°)
ZnO	3.248	5.196	0.390
ZnMnO	3.267	5.228	0.537

3.3. SEM morphological analysis

Fig. 5a and b show the SEM images of the ZnO in which nanostructures are detected. The sample also exhibits microgranular formation. This film is formed by rice-like structures with particle sizes of 300 to 800 nm and randomly distributed flower-like structures. The rice-like structures are in agreement with those reported on films obtained by CBD and SILAR methods [36,40,45]. Fig. 6a shows the SEM image for the ZnMnO, in which sheet-like structures with a lateral dimension of about 2 μm and a thickness of tens of nanometers can be seen. ZnMnO nanosheets are interconnected and have an approximately uniform size. A detailed SEM inspection of these samples showed that not only the aforementioned structures were found for the ZnMnO in Fig. 6b, but also that flower-like structures formed by interconnected hexagonal sheets of less than 5 μm can be seen. This kind of structures for the ZnMnO films was previously reported, when films were obtained by a pulsed electro-deposition-assisted chemical bath deposition method [33]. A very important point related to the SEM studies is that the Mn substitution on Zn sites strongly influenced the surface morphology of the film.

3.4. Semiquantitative EDS analysis

In order to determine that Mn is incorporated into the ZnO structure, an EDS analysis was performed. The semiquantitative composition of Mn in nanosheets was determined by EDS spectroscopy in 10 different sites. As a result, the Mn concentration had an average of 3.34 wt.%. Fig. 7 shows an EDS spectrum measured in one region of the sample. Values obtained for O, Si, Cl, Mn, and Zn are shown in Table 2. Cl could be observed in the composition of the film due to the precursor salts of Mn and Zn employed in the bath reaction. The peak labeled "*" originates from the Au layer for the SEM measurement.

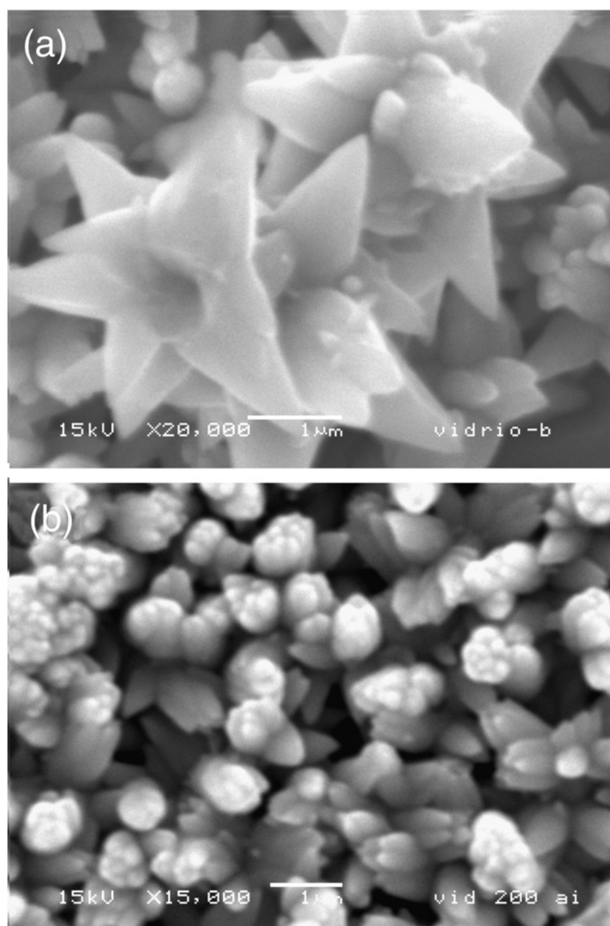

Fig. 5. SEM images of (a) flower-like and (b) rice-like structures of ZnO film.

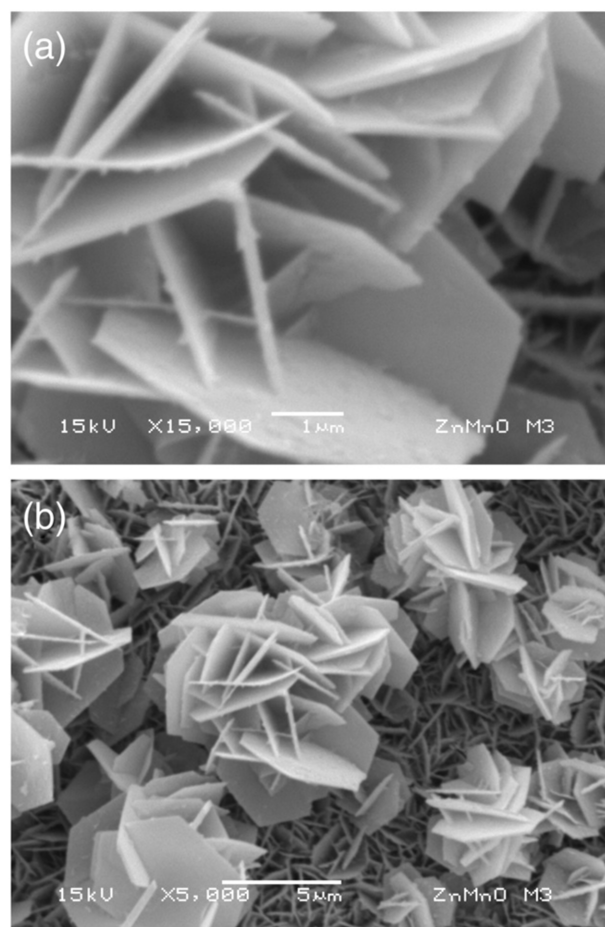

Fig. 6. SEM images of ZnMnO films: (a) details of smaller nanosheets in between flower-like structures, and (b) flower-like morphology.

3.5. Atomic force microscope (AFM)

An AFM was used to measure the surface roughness of the films over a 10 × 10 μm area by contact mode for ZnO and non contact mode for ZnMnO film. The 2D-AFM images of the surface morphology for ZnO and ZnMnO are shown in Fig. 8a and b. The surface topography of the films is indicative of the grain growth in the perpendicular

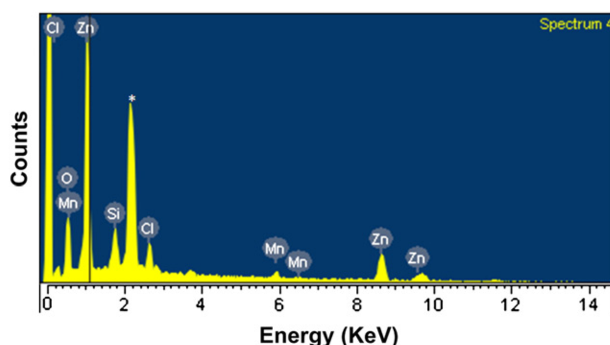

Fig. 7. EDS spectrum of ZnMnO film measured in one region.

Table 2
Values obtained from EDS spectra for ZnMnO film in one general region.

Element	Weight%	Weight% Standard deviation	Atomic%
O K	19.69	1.10	45.81
Si K	6.34	0.62	8.40
Cl K	6.69	0.55	7.03
Mn K	4.04	0.89	2.74
Zn L	63.24	1.29	36.02
Total	100.00		

direction to the substrate surface, which is in agreement with the XRD pattern. Compared to un-doped films, it was clearly observable that Mn increased the surface roughness. Un-doped films have a very smooth surface with a root mean square surface roughness of 83.9 nm, which agree well with the particle size of 300 to 800 for SEM images. This value increases to 217.5 nm for Mn doped film.

3.6. Atomic absorption results

The quantitative amount of Mn incorporated into ZnMnO films was determined by using atomic absorption spectroscopy. The manganese weight percentage calculated in the film was approximately 2.42%. This result is related to the one obtained from XRD using Vegard's law and by EDS, and confirms that Mn is incorporating less than 4%.

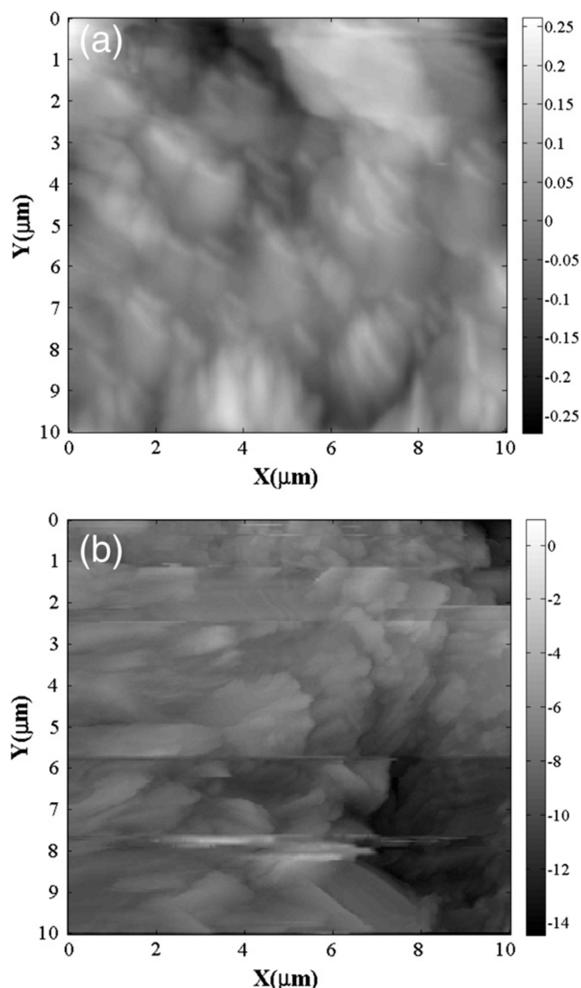

Fig. 8. AFM images of (a) ZnO and (b) ZnMnO films.

4. Conclusions

According to the aforementioned results, it is clear that by using the SILAR method, it is possible to obtain ZnO and ZnMnO films. The films consisted of a hexagonal phase with wurtzite structure of ZnO. The incorporation of manganese in ZnO films does not change the wurtzite structure but leads to the formation of nanosheet structure. Results obtained from EDS, Atomic absorption and XRD according Vegard's law allow us to conclude that less than 4% of Mn is incorporated into the ZnO structure. The morphology of ZnO films, constituted of rice-like and flower-like structures, changed significantly with the Mn incorporation, where nanosheets were formed. AFM images were used to find the surface roughness and confirm the presence of nanosheet structure revealed by SEM. In relation to the nanosheet structure, some studies have shown the presence of the dislocation lines in Mn-alloyed ZnO films along the c-axis [46]. The stress in the c-axis is caused by the Mn preferential inclusion in Zn sites. The experimental conditions allowed the growth on c-plane of hexagonal structures within substitutional Mn. The possible selective occupation of Mn in Zn sites and the concentration found in these thin films could be close to the percolation value of O–Mn through the whole structure.

Acknowledgments

This work was supported by both project PAPIIT 120809 UNAM, CONACYT 101332 México and COLCIENCIAS Colombia. The latter helps to support the work of F.N. Jiménez-García. Also, D. G. Espinosa-Arbeláez wants to thank CONACYT México for the financial support for PhD studies. C. Vargas-Hernandez wishes to thank the DIMA of Universidad Nacional de Colombia. This paper was revised by Translation Center at the Language Institute of the Universidad Autónoma de Manizales.

References

[1] R.R. Potter, Sol. Cells 16 (1986) 521.
[2] S.C. Ko, Y.C. Kim, S.S. Lee, S.H. Choi, S.R. Kim, Sens. Actuators A 103 (2003) 130.
[3] D.H. Yoon, G.M. Choi, Sens. Actuators B 45 (1997) 251.
[4] O.I. Lupan, S.T. Shishiyanu, T.S. Shishiyanu, Superlattices Microstruct. 42 (2007) 375.
[5] T.K. Gupta, J. Am. Ceram. Soc. 73 (1990) 1817.
[6] D.C. Look, Mater. Sci. Eng. B80 (2001) 383.
[7] Z.L. Wang, J. Phys. Condens. Matter 16 (2004) R829.
[8] X. Huang, G. Li, L. Duan, L. Li, X. Doua, L. Zhanga, Scr. Mater. 60 (2009) 984.
[9] T. Dietl, H. Ohno, F. Matsukura, J. Cibert, D. Ferrand, Science 287 (2000) 1019.
[10] W. Xu, Y. Zhou, X. Zhang, D. Chen, Y. Xie, T. Liu, W. Yan, S. Wei, Solid State Commun. 141 (2007) 374.
[11] A.C. Mofor, F. Reuss, A. El-Shaer, R. Kling, E. Schlenker, A. Bakin, H. Ahlers, U. Siegner, S. Sievers, M. Albrech, W. Schoch, W. Limmer, J. Eisenmenger, T. Mueller, A. Huebel, G. Denninger, P. Ziemann, A. Waag, Appl. Phys. A 88 (2007) 161.
[12] A. CheMofor, A. El-Shaer, A. Bakin, H.H. Wehmann, H. Ahlers, U. Siegner, S. Sievers, M. Albrecht, W. Schoch, N. Izyumskaya, V. Avrutin, J. Stoemenos, A. Waag, Superlattices Microstruct. 39 (2006) 381.
[13] E. Chikoidze, Y. Dumont, H.J. von Bardeleben, J. Gleize, F. Jomard, E. Rzepka, D. Ferrand, O. Gorochov, Appl. Phys. A88 (2007) 167.
[14] E. Chikoidze, Y. Dumont, H.J. von Bardeleben, J. Gleize, O. Gorochov, J. Magn. Magn. Mater. 316 (2007) e181.
[15] J. Gleize, E. Chikoidze, Y. Dumont, E. Rzepka, O. Gorochov, Superlattices Microstruct. 42 (2007) 242.
[16] S. Lee, H.S. Lee, S.J. Hwang, Y. Shon, D.Y. Kim, E.K. Kim, J. Cryst. Growth 286 (2006) 223.
[17] S. Lee, S.W. Lee, Y. Shon, D.Y. Kim, Mater. Sci. Eng. B 137 (2007) 40.
[18] S. Lee, Y. Shon, D.Y. Kim, Thin Solid Films 516 (2008) 4889.
[19] K. Masuko, A. Ashida, T. Yoshimura, N. Fujimura, J. Magn. Magn. Mater. 310 (2007) e711.
[20] S.K. Mandal, T.K. Nath, Thin Solid Films 515 (2006) 2535.
[21] W.Y. Shim, K.A. Jeon, K.I. Lee, S.Y. Lee, M.H. Jung, W.Y. Lee, J. Electron. Mater. 35–4 (2006) 635.
[22] T. Fukumura, Z. Jin, A. Ohtomo, H. Koinuma, M. Kawasaki, Appl. Phys. Lett. 75 (1999) 3366.
[23] W. Chen, J. Wang, M.R. Wang, Vacuum 81 (2007) 894.
[24] J. Wang, W. Chen, M.R. Wang, J. Alloys Compd. 449 (2008) 44.
[25] G. Srinivasan, J. Kumar, J. Cryst. Growth 310 (2008) 1841.
[26] J.H. Li, D.Z. Shen, J.Y. Zhang, D.X. Zhao, B.S. Li, Y.M. Lu, Y.C. Liu, X.W. Fan, J. Lumin. 122–123 (2007) 352.
[27] A.E. Jiménez-Gónzalez, J. Solid State Chem. 128 (1997) 176.
[28] G.A. Mohamed, A.B. Abd El-Moiz, M. Rashad, Physica B 370 (1–4) (2005) 158.

[29] S.T. Shishiyanu, O.I. Lupan, E.V. Monaico, V.V. Ursaki, T.S. Shishiyanu, I.M. Tiginyanu, Thin Solid Films 488 (2005) 15.
[30] C.H. Ye, Y. Bando, G.Z. Shen, D. Goldberg, J. Phys. Chem. C 110 (2006) 15146.
[31] M. Fukarova-Jurukovska, M. Ristov, A. Andonovski, Thin Solid Films 299 (1997) 149.
[32] E.S. Jang, J.H. Won, S.J. Hwang, J.H. Choy, Adv. Mater. 18 (2006) 3309.
[33] X. Huang, G. Li, L. Duan, L. Li, X. Dou, L. Zhang, Scr. Mater. 60 (2009) 984.
[34] C. Vargas-Hernández, F.N. Jiménez-Garcia, J.F. Jurado, Microelectron. J. 39 (2008) 1349.
[35] P. Mitra, J. Khan, Mater. Chem. Phys. 98 (2006) 279.
[36] X.D. Gao, X.M. Li, W.D. Yu, J. Solid State Chem. 177 (2004) 3830.
[37] J.W. Mellor, A Comprehensive Treatise on Inorganics and Theoretical Chemistry, vol. 4, Longman, NY, USA, 1946, p. 521.
[38] C.C. Lin, Y.Y. Li, Chem. Eng. J. 144 (2008) 509.
[39] Z.B. Bahsi, A.Y. Oral, Opt. Mater. 29 (2007) 672.
[40] A.P. Chaterje, P. Mitra, A.K. Mukhopadhyay, J. Mater. Sci. 34 (1999) 4225.
[41] A.E. Jimenez Gonzales, P.K. Nair, Semicond. Sci. Technol. 10 (1995) 1277.
[42] Y.M. Kim, M. Yoon, I.-W. Park, Y.J. Park, Jong H. Lyou, Solid State Commun. 129 (2004) 175.
[43] S.K. Hong, H.J. Ko, Y. Chen, T. Yao, J. Cryst. Growth 209 (2000) 537.
[44] J.K. Furdyna, J. Appl. Phys. 64 (1988) R29.
[45] P.S. Kumar, A.D. Raj, D. Mangalaraj, D. Nataraj, Appl. Surf. Sci. 255 (2008) 2382.
[46] M. Diaconu, H. Schmidt, H. Hochmuth, M. Lorenz, G. Benndorf, D. Spemann, A. Setzer, P. Esquinazi, A. Pöppl, H. von Wenckstern, K.-W. Nielsen, R. Gross, H. Schmid, W. Mader, G. Wagner, M. Grundmann, J. Magn. Magn. Mater. 307 (2006) 212.